Supplementary material: Descending, lifting or smoothing: Secrets of robust cost optimization

Christopher Zach[1] and Guillaume Bourmaud[2]

[1] Toshiba Research Europe, Cambridge, United Kingdom
[2] University of Bordeaux, Bordeaux, France

1 Supplementary material of Sec. 5: The first order expansion of $(\gamma'(w))^2/\gamma(w)$ at $w = 1$

Using l'Hospital's rule we obtain

$$\begin{aligned}\lim_{w\to 1} \frac{w(\gamma')^2}{\gamma} &:= \lim_{w\to 1} \frac{N(w)}{D(w)} = \lim_{w\to 1} \frac{N'(w)}{D'(w)} \\ &= \lim_{w\to 1} \frac{(\gamma')^2 + 2w\gamma'\gamma''}{\gamma'} = \lim_{w\to 1} \gamma' + 2w\gamma'' = 2\gamma''(1).\end{aligned}$$

By applying the quotient rule we have to calculate (omitting the argument w)

$$\begin{aligned}\lim_{w\to 1} \left(\frac{(\gamma')^2}{\gamma}\right)' &= \lim_{w\to 1} \frac{\gamma'(2\gamma''\gamma - (\gamma')^2)}{\gamma^2} \\ &= \lim_{w\to 1} \frac{\gamma''(2\gamma''\gamma - (\gamma')^2) + \gamma'(2\gamma\gamma''' + 2\gamma'\gamma'' - 2\gamma'\gamma'')}{2\gamma'\gamma} \\ &= \lim_{w\to 1} \frac{\gamma''(2\gamma''\gamma - (\gamma')^2) + 2\gamma\gamma'\gamma'''}{2\gamma'\gamma} \\ &= \lim_{w\to 1} \frac{\gamma''(2\gamma\gamma'' - (\gamma')^2)}{2\gamma\gamma'} + \gamma'''(1) =: A + \gamma'''(1). \qquad (1)\end{aligned}$$

We cannot separate the numerator in the first term, as it is of indeterminate "$\infty - \infty$" form. We call the first term A and continue to apply l'Hospital's rule,

$$\begin{aligned}A &= \lim_{w\to 1} \frac{\gamma'''(2\gamma\gamma'' - (\gamma')^2) + \gamma''(2\gamma'\gamma'' + 2\gamma\gamma''' - 2\gamma'\gamma'')}{2((\gamma')^2 + \gamma\gamma'')} \\ &= \lim_{w\to 1} \frac{\gamma'''(2\gamma\gamma'' - (\gamma')^2) + 2\gamma\gamma''\gamma'''}{2((\gamma')^2 + \gamma\gamma'')} = \frac{\gamma'''(1)}{2} \lim_{w\to 1} \frac{4\gamma\gamma'' - (\gamma')^2}{(\gamma')^2 + \gamma\gamma''} \\ &= \frac{\gamma'''(1)}{2} \lim_{w\to 1} \frac{4\gamma'\gamma'' + 4\gamma\gamma''' - 2\gamma'\gamma''}{2\gamma'\gamma'' + \gamma'\gamma'' + \gamma\gamma'''} = \gamma'''(1) \lim_{w\to 1} \frac{\gamma'\gamma'' + 2\gamma\gamma'''}{3\gamma'\gamma'' + \gamma\gamma'''} \\ &= \frac{\gamma'''(1)}{3} \lim_{w\to 1} \frac{3\gamma'\gamma'' + 6\gamma\gamma'''}{3\gamma'\gamma'' + \gamma\gamma'''} = \frac{\gamma'''(1)}{3} \left(1 + \lim_{w\to 1} \frac{5\gamma\gamma'''}{3\gamma'\gamma'' + \gamma\gamma'''}\right)\end{aligned}$$

$$= \frac{\gamma'''(1)}{3}\left(1 + \lim_{w\to 1}\frac{5(\gamma'\gamma''' + \gamma\gamma'''')}{3(\gamma'')^2 + 3\gamma'\gamma''' + \gamma'\gamma''' + \gamma\gamma''''}\right)$$
$$= \frac{\gamma'''(1)}{3}\left(1 + \frac{5\cdot 0}{3(\gamma''(1))^2 + 0}\right) = \frac{\gamma'''(1)}{3}, \tag{2}$$

as the denominator is non-zero. Overall we obtain

$$\lim_{w\to 1}\left(\frac{(\gamma')^2}{\gamma}\right)' = \gamma'''(1) + A = \frac{4}{3}\gamma'''(1) \tag{3}$$

and the first order expansion of $w \mapsto (\gamma'(w))^2/\gamma(w)$ at $w = 1$ is given by

$$\frac{(\gamma'(1+\Delta v))^2}{\gamma(1+\Delta v)} \approx 2\gamma''(1) + \tfrac{4}{3}\gamma'''(1)\Delta v. \tag{4}$$

The first order expansion of the mapping $u \mapsto (w'(u))^2/w(u)$ around 0 is derived analogously.

2 Supplementary material of Sec. 6: Proof of Lemma 2

We restate the lemma for convenience: let $\eta \in (0,1)$. If $\rho^k_\Psi \geq \frac{\eta+1}{2\eta} > 0$ or $\rho^k_\Psi \leq \frac{\eta-1}{2\eta} < 0$ then $\rho^k_\Delta \leq \eta$.

The first case: $\rho^k_\Psi \geq \frac{\eta+1}{2\eta} > 0$: Expanding and rearranging we terms read

$$(\eta+1)\left(\Delta^k_\leq - \Delta^k_>\right) \leq 2\eta\left(\Delta^{k-1}_\leq - \Delta^{k-1}_>\right) \leq 2\eta\left(\Delta^k_\leq - \Delta^{k-1}_>\right) \leq 2\eta\Delta^k_\leq,$$

where we used Lemma 1 and that $\Delta^{k-1}_> \geq 0$. Consequently,

$$(\eta+1)\Delta^k_\leq - (\eta+1)\Delta^k_> \leq 2\eta\Delta^k_\leq$$

or

$$\Delta^k_\leq - \Delta^k_> \leq \eta\left(\Delta^k_\leq + \Delta^k_>\right), \tag{5}$$

therefore $\rho^k_\Delta \leq \eta$. The second case is similar: $\rho^k_\Psi \leq \frac{\eta-1}{2\eta} < 0$ means that

$$(\eta-1)\left(\Delta^k_\leq - \Delta^k_>\right) \geq 2\eta\left(\Delta^{k-1}_\leq - \Delta^{k-1}_>\right) \geq 2\eta\left(\Delta^k_\leq - \Delta^k_>\right) \geq -2\eta\Delta^k_>$$

(again using Lemma 1 and $\Delta^k_\leq \geq 0$), i.e.

$$-\Delta^k_\leq + \Delta^k_> \geq -\eta(\Delta^k_\leq + \Delta^k_>) \tag{6}$$

and therefore $\rho^k_\Psi \leq \frac{\eta-1}{2\eta}$.

3 Details on the weak membrane energy and visual results

The starting point of our weak membrane energy is the following objective: let $\mathbf{u} \in [0,1]^{|\mathcal{V}|}$ be a given observed image (with normalized image intensities), then

$$\Psi^{\text{Membrane}}(\boldsymbol{\theta}; \mathbf{u}) = \tfrac{\lambda}{2} \sum\nolimits_{i \in \mathcal{V}} \min\{\nu, (\theta_i - u_i)^2\} + \sum\nolimits_{(i,j) \in \mathcal{E}} \min\{\mu, (\theta_i - \theta_j)^2\}. \tag{7}$$

We replace the hard truncated quadratic costs by an arbitrary robust kernel ψ with bound range as described below. We set $\lambda = 1$, $\nu = 1/5$ and $\mu = 1/200$ for the results below.

Fitting a robust kernel to a truncated quadratic cost: Let $\hat{\psi}(x) = \min\{\eta, |x|\}^2/2 = \min\{\eta^2, x^2\}/2$ and ψ be a bounded kernel with $\psi_\infty := \lim_{x \to \infty} \psi(x) < \infty$. We want to rescale ψ to obtain $\tilde{\psi}$ such that $\tilde{\psi}_\infty = \hat{\psi}_\infty = \eta^2/2$ and $\tilde{\psi}''(0) = 1$. $\tilde{\psi}$ is modeled as $\tilde{\psi}(x) = \alpha\psi(x/\tau)$ for parameters α and τ to be determined. We have

$$\tilde{\psi}''(0) = (\tilde{\psi}(x))''|_{x=0} = \frac{\alpha}{\tau^2}\psi''(x/\tau)|_{x=0} = \frac{\alpha}{\tau^2} \stackrel{!}{=} 1$$
$$\tilde{\psi}_\infty = \lim_{x \to \infty} \alpha\psi(x/\tau) = \alpha\psi_\infty \stackrel{!}{=} \eta^2/2,$$

from which we deduce that $\alpha = \eta^2/(2\psi_\infty)$ and $\tau^2 = \alpha = \eta^2/(2\psi_\infty)$. Hence, $\tilde{\psi}$ is given by

$$\tilde{\psi}(x) = \frac{\eta^2}{2\psi_\infty}\psi\left(\frac{\sqrt{2\psi_\infty}x}{\eta}\right) = \tau^2\psi\left(\frac{x}{\tau}\right) = \psi_\tau(x),$$

with $\tau = \eta/\sqrt{2\psi_\infty}$.

3.1 Visual results for the weak membrane energy

In Figs. 1 and 2 we visualize the solutions returned by the various methods. The input image is the clean image with 10% of pixels replaced by uniformly sampled intensity values from $[0, 1]$. The initial point $\boldsymbol{\theta}^0$ is an image with uniformly sampled intensity values. As expected, IRLS performs very poorly, and all other methods yield very similar results. Interestingly, the lifted Gauss-Newton approach keeps a few noisy pixels (although the reached objective is not falling behind), which suggests that there are different biases in the methods, that determines which of the essentially equivalent solutions are actually returned.

Further, Fig. 3 illustrates the evolution of objectives for the "Marilyn" image and is therefore analogous to Fig. 3 in the main text.

(a) Noisy input (b) IRLS (c) l-G-N (d) l-Newton (e) GOM+

Fig. 1: Visual results for the "Lena" image.

(a) Noisy input (b) IRLS (c) l-G-N (d) l-Newton (e) GOM+

Fig. 2: Visual results for the "Marilyn" image.

4 Datasets used for robust bundle adjustment

The datasets are in particular `ladybug-318`, `ladybug-598`, `trafalgar-138`, `trafalgar-257`, `dubrovnik-150`, `dubrovnik-356`, `venice-245`, `venice-427`, `final-93` and `final-394`.

5 Variational stereo and the limits of half-quadratic lifting

Since the lifted methods (such as lifted Gauss-Newton) are very competitive for a weak membrane model, we use a similar formulation for dense disparity estimation. We use a 3×3 ZNCC matching cost to obtain a cost profile, from which

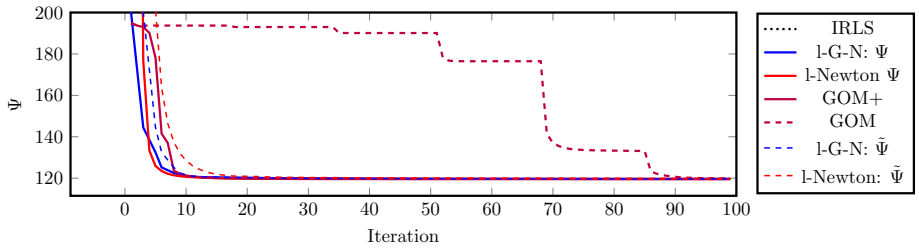

Fig. 3: Evolution of Ψ^{Membrane} w.r.t. the number of iterations for the "Marilyn" image. We plot the target cost Ψ and lifted one $\tilde{\Psi}$ for the lifting based methods.

K_i (at most 5) local minima per pixel i in the reference image are extracted. $d_{i,k}$ denotes the disparity of the k-th local minimum (sorted w.r.t. the matching cost). Similar to the weak membrane model the underlying cost contains robust data and smoothness terms:

$$\Psi^{\text{Stereo}}(\boldsymbol{\theta}; \mathbf{d}) = \frac{\lambda}{2} \sum\nolimits_{i \in \mathcal{V}} \sum_{k=1}^{K_i} \psi_{\text{data}}(\theta_i - d_{i,k}) + \sum\nolimits_{(i,j) \in \mathcal{E}} \psi_{\text{smooth}}(\theta_i - \theta_j). \quad (8)$$

The robust optimization methods are initialized with the best cost (local matching) solution (depicted in Fig. 4(a) and (d)). In this application lifting-based approaches perform poorly, where the estimated solution stays very close to its initialization (as seen in Figs. 4(b,e)). Graduated optimization (using the GOM+ variant) leads to sensible (although not entirely perfect) solutions. The evolution of robust costs w.r.t. the number of solver iterations is shown in Fig. 5. Although the objective Ψ^{Stereo} has a structure very similar to the weak membrane cost Ψ^{Membrane}, the lifting-based methods perform only slightly better than IRLS in the stereo example (i.e. both IRLS and lifting methods are essentially stuck near the initial solution).

In order to investigate the poor performance of half-quadratic lifting, we successively adapted the setting to match the weak membrane case: (i) using a random initialization (instead of the best cost solution), or (ii) setting $K_i = 1$ for all i (thus reducing the number of local minima in the objective). The lifted approach becomes competitive again (and far superior to IRLS) once (i) and (ii) are active (see Figs. 6 and 7). Characterizing the set of problem instances, where a particular method for robust cost minimization performs well (or is likely to fail), is therefore a challenging direction for future research.

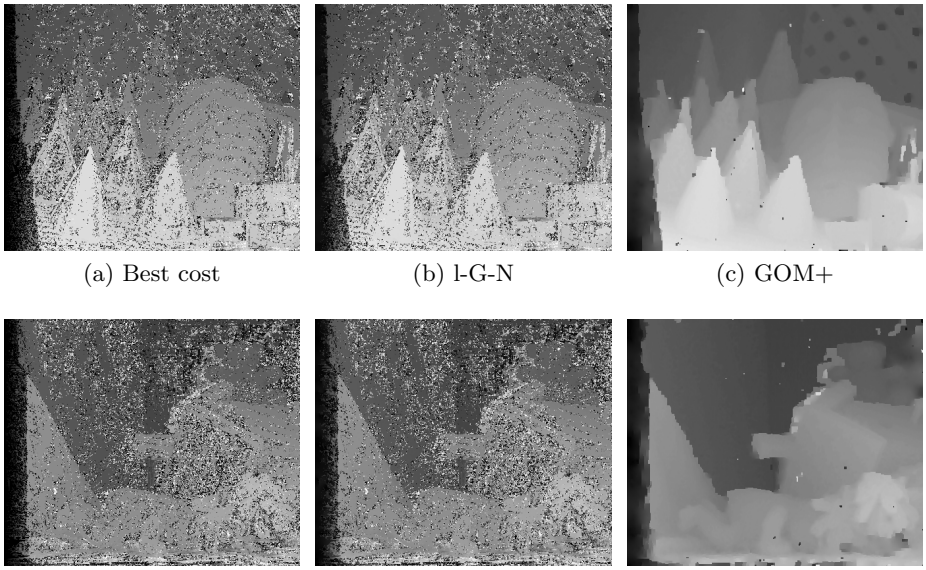

(a) Best cost (b) l-G-N (c) GOM+

(d) Best cost (e) l-G-N (f) GOM+

Fig. 4: Visual results for the "variational stereo" approach using best cost initialization and $K_i = 5$.

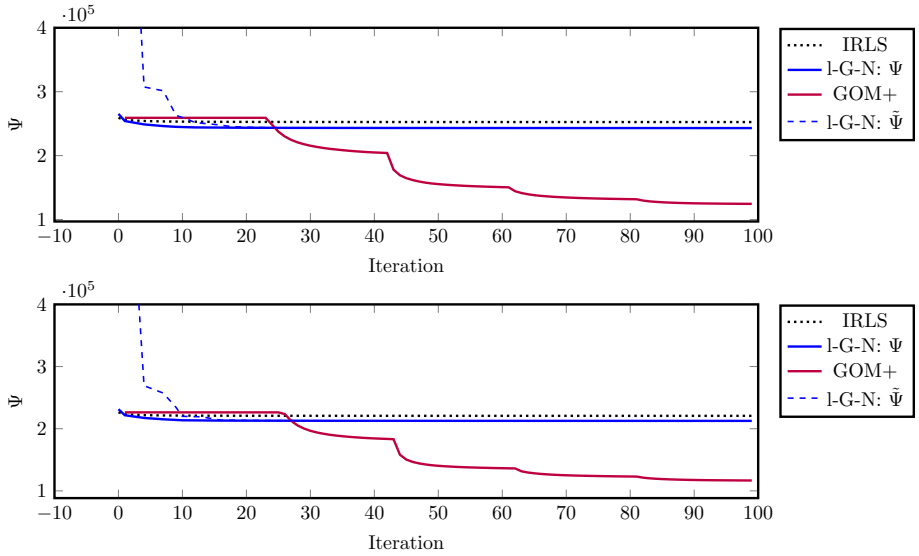

Fig. 5: Evolution of Ψ^{stereo} w.r.t. the number of iterations for the "teddy" and "cones" stereo image pair. We plot the target cost Ψ and lifted one $\tilde{\Psi}$ for the lifting Gauss-Newton method.

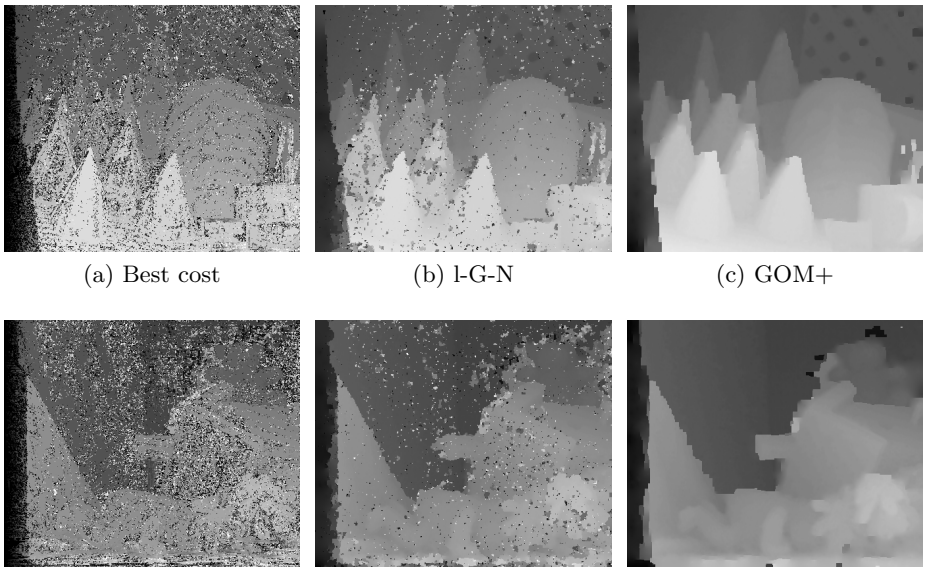

(a) Best cost (b) l-G-N (c) GOM+

(d) Best cost (e) l-G-N (f) GOM+

Fig. 6: Visual results for the "variational stereo" approach using random initialization and $K_i = 1$.

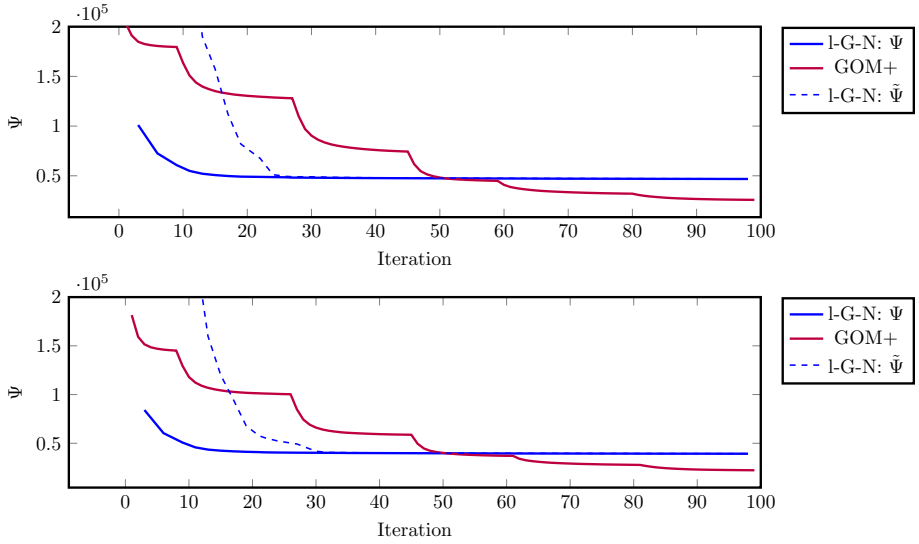

Fig. 7: Evolution of Ψ^{stereo} w.r.t. the number of iterations for the "teddy" and "cones" stereo image pair (random initialization and $K_i = 1$). We plot the target cost Ψ and lifted one $\tilde{\Psi}$ for the lifting Gauss-Newton method.